γ-ray generation enhancement by the charge separation field in laser-target interaction in the radiation dominated regime

R. Capdessus, M. Lobet, E. d'Humières, and V. T. Tikhonchuk

Citation: Physics of Plasmas (1994-present) **21**, 123120 (2014); doi: 10.1063/1.4904813
View online: http://dx.doi.org/10.1063/1.4904813
View Table of Contents: http://scitation.aip.org/content/aip/journal/pop/21/12?ver=pdfcov
Published by the AIP Publishing

γ-ray generation enhancement by the charge separation field in laser-target interaction in the radiation dominated regime

R. Capdessus,[1,2] M. Lobet,[2,3] E. d'Humières,[2] and V. T. Tikhonchuk[2]
[1]*Department of Physics SUPA, University of Strathclyde, Glasgow G4 0NG, United Kingdom*
[2]*University of Bordeaux - CNRS - CEA, CELIA, UMR 5107, F-33400 Talence, France*
[3]*CEA, DAM, DIF, F-91297, Arpajon, France*

(Received 18 June 2014; accepted 8 December 2014; published online 30 December 2014)

A new source of radiation can be created with a laser pulse of intensity $\approx 10^{23}$ W/cm^2 interacting with a slightly overdense plasma. Collective effects driven by the electrostatic field significantly enhance the synchrotron radiation. They impact on the laser energy repartition leading to a specific emission but also constitute a crucial element for the intense radiation production. They allow electrons to be accelerated over a length up to 10 laser wavelengths favoring emission of an intense radiation. It is shown that charge separation field depends on the ion mass and target thickness but also on laser polarization. These phenomena are studied with an one dimensional relativistic particle-in-cell code accounting for the classical radiation reaction force.
 [http://dx.doi.org/10.1063/1.4904813]

I. INTRODUCTION

Recent theoretical studies of a high intensity laser pulse interaction with matter advocate new schemes of acceleration of charged particles, electrons and ions, to relativistic energies.[1] Generation of intense fluxes of γ-rays is also expected.[2] These theoretical studies lay a solid background for experiments planned with new laser installations such as the ELI (Extreme Light Infrastructure) project,[3] which is expected to produce a peak power above 100 PW with an energy ∼500 J. This will permit to study new physical regimes where the charge separation field plays an important role and which have never been explored in experiment. This is very promising for many applications, as in the cancer therapy, radiography, and fast ignition of inertial fusion reactions.[4] Besides, it has been shown in several publications that the radiation reaction force acting on ultrarelativistic electrons accelerated in the strong laser fields intensities above 10^{22} W/cm^2 will strongly impact their dynamics.[2,5–13] It has been demonstrated that the radiation reaction force leads to a contraction of the electron phase space volume with time, localized in the ambient laser field, in the case of non-interacting electrons.[9,14] Nevertheless, the use of kinetic theory to describe non-interacting electrons has been criticized in Ref. 15 due to non-Hamiltonian nature of the Landau-Lifshitz equation. However, it has been demonstrated in Refs. 16 and 17 that conclusions of Ref. 15 are injustified and that the Vlasov equation with the radiation reaction accounted for is as consistent as the Vlasov equation with the Lorentz force.

The possibility to detect radiation reaction effects has been studied in Refs. 2, 12, and 18–20. However, up to now the studies of synchrotron radiation did not consider the role of the collective field related to self-consistent electric fields in plasma. Other phenomena such as turbulence, instabilities can also contribute to an enhancement of collective effects. Here, we restrain our study only to the charge separation field effects and neglect other phenomena. The goal of this paper is to demonstrate a strong feedback of the plasma collective effects on the synchrotron radiation. The collective effects increase with the ion mass and target thickness, and they are crucial for converting a significant fraction of the laser energy into an intense radiation.

The paper is organized as follows. Section II briefly gathers three fundamental points: an analysis of the electron equation of motion, a comment on the role of the electrostatic field, and an analysis on the synchrotron radiation. Section III is devoted to the numerical approach where the synchrotron radiation computation algorithm is described and the simulation parameters are given. Sections IV–VII are devoted to studies of various regimes of laser plasma interaction. Section IV describes the dependence of the laser absorption on the target thickness. Section V is devoted to studies of the influence of the charge separation field on electron acceleration and conditions of the intense radiation production. Section VI considers several setups of practical interest where the charge separation field has a significant influence on radiation emission. The temporal and spatial behavior is analyzed and the emitted radiation is studied by variation of the laser polarization, the target thickness, and the ion mass. Finally in Sec. VII, the validity of the classical approach is proved in comparisons with the quantum electrodynamics (QED) Monte Carlo modelling.[21]

II. THEORETICAL APPROACH

A. Electron dynamic equations

In order to take into account the radiation reaction force, we use the renormalized Lorentz-Abraham-Dirac (LAD) equation[22] recently derived by Sokolov.[23] Compared to Landau-Lifshitz approach,[24] it conserves the four-vector of energy-momentum of the electron and it is more convenient

for the numerical implementation. We define the dimensionless laser amplitude

$$a_L = \frac{eE_L}{m_e c\omega_L} \gg 1, \tag{1}$$

and the radiation parameter

$$a_L \omega_L \tau_r \ll 1. \tag{2}$$

Here, ω_L is the laser frequency and $\tau_r = e^2/6\pi\epsilon_0 m_e c^3 \simeq 6.2\times10^{-24}$ s is the characteristic radiation time. The dimensionless laser amplitude a_L is of the order of 100 in the domain of our interest and the parameter $a_L\omega_L\tau_r$ is assumed to be small ($\sim10^{-6}$). So the quantum effects in the electron radiation process can be neglected. This statement is confirmed in Sec. VII. In the second order in $a_L\omega_L\tau_r$ the equations of electron motion read[23]

$$\dot{\mathbf{p}}_e = \mathbf{F}_{Le} - ec\,\boldsymbol{\delta\beta}_e \times \mathbf{B} - \gamma_e^2(\mathbf{F}_{Le}\cdot\boldsymbol{\delta\beta}_e)\boldsymbol{\beta}_e, \tag{3}$$

$$\dot{\mathbf{x}}_e = c(\boldsymbol{\beta}_e + \boldsymbol{\delta\beta}_e), \tag{4}$$

where

$$\boldsymbol{\delta\beta}_e = \frac{\tau_r}{m_e c}\frac{\mathbf{F}_{Le} - (\mathbf{F}_{Le}.\boldsymbol{\beta}_e)\boldsymbol{\beta}_e}{1 + \frac{\tau_r}{m_e c}(\mathbf{F}_{Le}.\boldsymbol{\beta}_e)}, \tag{5}$$

is the radiation correction to the electron velocity and $\mathbf{F}_{Le} = -e(\mathbf{E} + \mathbf{v}_e \times \mathbf{B})$ is the Lorentz force.

The associated invariant parameter characterizes the importance of the quantum effects

$$\chi_e = \frac{e\hbar\gamma_e}{m_e^2 c^3}\sqrt{(\mathbf{E} + \boldsymbol{\beta}_e \times \mathbf{B})^2 - (\boldsymbol{\beta}_e \cdot \mathbf{E})^2} \propto \sqrt{\delta\boldsymbol{\beta}_e.\mathbf{F}_{Le}}. \tag{6}$$

This is a ratio of the electric field in the electron rest frame and the Schwinger field $E_{sch} = m_e c^2/e\lambda_c$ where $\lambda_c = h/m_e c$ is the Compton length. In the case of a plane laser wave $\chi_e = \gamma_e(1-\beta_{e\|})a_L\hbar\omega_L/m_e c^2$ depends on the dimensionless laser amplitude a_L and on the projection of the electron velocity on the laser wave vector direction $\beta_{e\|}$. The so-called classical regime refers to the case where $\chi_e \ll 1$, so that the quantum electrodynamics effects on the emission can be neglected. In this case, a continuous treatment of the radiation losses according to the Sokolov approach is well suited. At higher laser intensities where $\chi_e \sim 1$, the quantum nature of the radiation, with emission of photon with the energy comparable to the electron energy, leads to discontinuous particle trajectories with significant recoils. Then the Monte-Carlo description[21,25,26] is more appropriate. In the semi-classical regime $\chi_e \sim 0.1$, a continuous treatment of the emission is still possible, although the expressions for the total radiated power and spectrum need to be corrected.[27,28]

B. Electrostatic field

In the laser-plasma interaction, the electrons are pushed by the ponderomotive force thus creating a charge separation field, E_s. The importance of the latter can be characterized by the parameter α

$$\alpha \equiv \frac{E_s(t)}{E_L}, \tag{7}$$

which is the ratio of the electrostatic field to the laser electric field in a target. In order to ensure strong charge separation field, we need $\alpha \sim 1$. In the case of a thin target, $l \sim \lambda_L$, this can be achieved under the condition $\kappa \equiv \pi\frac{n_e}{n_c}\frac{l}{\lambda_L}\frac{1}{a_L} \sim 1$ which can be seen as a threshold for relativistic self-induced transparency regime (see Ref. 29). Here, l is the target thickness n_e is the electron plasma density, $n_c = \omega_L^2 m_e\epsilon_0/e^2$ is the critical density, and $\lambda_L = 2\pi c/\omega_L$ is the laser wavelength. In the case of a thick target, $l \gg \lambda_L$, the charge separation field can be observed at the front target surface if the following condition is fulfilled:

$$\frac{n_e}{n_c} \ll a_L. \tag{8}$$

C. Synchrotron radiation

The electron synchrotron emission is responsible for the radiation produced by an ultra-intense laser pulse interacting with a low density plasma. The power, P_r, radiated by one ultra-relativistic electron in the first order expansion on the small parameter $a_L\omega_L\tau_r$ reads[30]

$$\frac{d^2P_r}{d\omega d\boldsymbol{\Omega}} = \gamma_e^2\frac{\tau_r}{m_e}\mathbf{F}_{Le}^2\left(1 - \cos^2\psi\beta_e^2\right)\boldsymbol{\delta}\left(\boldsymbol{\Omega} - \frac{\mathbf{p}_e}{p_e}\right)S\left(\frac{\omega}{\omega_{cr}}\right). \tag{9}$$

Here, ψ is the angle between the laser electric field and the electron velocity. The function $S(r) = 3^{5/2}(8\pi)^{-1}r\int_r^\infty K_{5/3}r'dr'$ describes the normalized spectrum, which depends on the Macdonald's function, $K_{5/3}$ and on the critical frequency $\omega_{cr} = 3/2\gamma_e^3||\mathbf{F}_{Le}\times\mathbf{p}_e||/||\mathbf{p}_e||^2$ (see Ref. 24). The radiation is emitted in a narrow cone with the angle $\sim 1/\gamma_e \ll 1$ with respect to the electron propagation direction. This is formalized by a Dirac function δ, in Eq. (9). The total radiation energy is calculated as a sum of all electrons in the simulation box. Originally, the synchrotron radiation corresponds to the emission of an electron in a homogeneous magnetic field. Here, this notion is applied in a more general sense as an emission of a relativistic electron in a combined laser and self-consistent plasma electromagnetic fields.

The total power radiated by electrons from a unit plasma volume is defined as follows:

$$W_\gamma = \int_{\mathbb{R}^3} d\mathbf{p}_e f_e \gamma_e^2 \frac{\tau_r}{m_e}F_{Le}^2\left(1 - \cos\psi^2\frac{\gamma_e^2 - 1}{\gamma_e^2}\right), \tag{10}$$

where f_e is the electron distribution function with $\int_{\mathbb{R}^3} f_e d\mathbf{p}_e = n_e$. In the case of a Maxwell-Juttner distribution and assuming $\gamma_e \sim a_L(g+\alpha^2)^{1/2}$ and $T_e \simeq a_L m_e c^2$ (see Ref. 31), expression (10) leads to

$$W_\gamma \simeq 6(g+\alpha^2)^2 n_e a_L^4 \tau_r \omega_L m_e c^2 \omega_L, \tag{11}$$

where the function $g(t)$ describes the laser pulse shape and $\int_0^\infty g(t)\mathrm{d}t = \tau_L$ is the laser pulse duration.

The intensity of synchrotron emission of an electron in a strong laser field, $a_L \gg 1$, is proportional to the fourth power of the laser amplitude, $P_r \sim m_e c^2 \omega_L^2 \tau_r a_L^4$.[24] It is much more intense than the Bremsstrahlung emission which for an electron with the energy $\gamma_e m_e c^2$ in a plasma with an ion density n_i can be estimated as:[32] $P_B \simeq \frac{Z}{\pi}\frac{1}{137}\sigma_T n_i m_e c^3 \gamma_e$, where σ_T is the Thomson cross section and Z is the ion charge. Assuming $Z \sim 1$, the electron energy defined by the laser field, $a_L \sim \gamma_e$ and $n_i \sim n_e \sim n_c$, one finds that the Bremsstrahlung radiation is negligible compared to the synchrotron emission for laser amplitudes $a_L \geq 100$.

The radiation dominated regime is defined by the condition that the photon energy emitted during one laser period by an electron is larger than the electron energy[6]

$$\frac{P_r}{\omega_L} \gtrsim \gamma_e m_e c^2. \tag{12}$$

For $\gamma_e \sim a_L$, and $P_r \sim m_e c^2 \omega_L^2 \tau_r a_L^4$, the condition (12) writes as $a_L^3 \omega_L \tau_r \sim 1$ which corresponds to the laser amplitude $a_L \sim 440$ or to the laser intensity $I_L \simeq 2.7 \times 10^{23}\,\mathrm{W/cm^2}$.

In the case of a radiating plasma, we have to take into account both the electrostatic field E_s and the laser field E_L. Then, the condition (12) for a unit plasma volume can be rewritten as:

$$\frac{W_\gamma}{\omega_L} \geq n_e \gamma_e m_e c^2. \tag{13}$$

Using the expression (11), it yields

$$a_L \geq \left(\frac{1}{6\omega_L \tau_r}\right)^{1/3} \left(\frac{1}{1+\alpha^2}\right)^{3/2}. \tag{14}$$

The comparison of Eqs. (12) and (14) shows a difference between the case of one electron and a plasma, where the threshold of the radiation dominated regime may be reduced by a factor of 3–5.

III. NUMERICAL APPROACH

A. Radiation computation

Particle-In-Cell (PIC) codes provide a good description of plasma dynamics with a reasonable precision and in an acceptable computing time. In particular, PIC codes are useful to study collective effects in plasma which dominate at ultra-high laser pulse intensities. The radiation losses and the radiation reaction force have been implemented in the PIC code PICLS.[33] We use a fourth-order interpolation for the numerical solver presented in Ref. 11, to apply fields and to deposit currents. The time step Δt is linked to the mesh size Δx by a simple relation: $\Delta x = c\Delta t$, where c is the light velocity. The numerical implementation of radiation losses has been discussed in Refs. 7 and 11. The radiation force is calculated with the same pusher that calculates the Lorentz force. This additional calculation does not affect the stability of the numerical scheme. The radiation is computed from the macro-particle trajectories assuming the emission to be incoherent. This means that the characteristic distance between electrons, $d \sim n_e^{-1/3}$ is greater than the radiation wavelength, $\lambda_\gamma = 2\pi c/\omega$, for every radiating electron. The incoherence condition can be expressed as follows:

$$\frac{2\pi c}{\omega_\gamma} \ll n_e^{-1/3}, \tag{15}$$

which leads to cutoff condition on the photon spectrum

$$\hbar\omega \gg 2.75 \left(\frac{n_e}{n_c}\right)^{1/3} \lambda_{L,[\mu m]}^{-2/3}\,\mathrm{keV}. \tag{16}$$

In the particular case of $n_e = 10 n_c$ and $\lambda_L = 1\,\mu$m, this condition corresponds to the cutoff at $\simeq$1.2 keV. In addition, Eqs. (10) and (9) imply that the electron trajectory at each time step can be approximated by an arc. Thus, the angular variation of the electron momentum must be less than $1/\gamma_e$ at the computational time step, Δt. Considering the instantaneous electron rotation frequency (see Refs. 24 and 32), $\omega_{re} = ||\mathbf{p}_e \times \mathbf{F}_{Le}||/p_e^2 \sim \frac{a_L}{\gamma_e}\omega_L$, this imposes the following condition $\frac{\omega_{re}}{2\pi}\Delta t < 1/\gamma_e$:

$$\Delta t \leq \frac{T_L}{a_L}. \tag{17}$$

We choose a cell size such that $\Delta x = \lambda_L/300$ fulfilling the condition (17). Each plasma cell contains 100 macroparticles, electrons, and ions. The numerical stability of the particle pusher including radiation friction force has been studied in several test runs with the same number of macroparticles per mesh but with a smaller time steps $\Delta t = T_L/500$ and $\Delta t = T_L/1000$. No significant changes have been observed, in the particle dynamics and in radiation, which confirms the validity of condition (17). We consider a grid of 1000 cells in the photon energy over the range $10^{-3}\mathrm{MeV} \leq \hbar\omega \leq 10^{3}\mathrm{MeV}$ in agreement with condition (16), 90 cells in the polar angle θ over the range $0 \leq \theta \leq 2\pi$. The polar axis is defined along the laser propagation direction. These numerical parameters enable a compromise between a good precision, a minimum noise and a reasonable calculation time.

In order to observe strong collective effects, the electrostatic field amplitude has to be of the same magnitude as the laser field. It is therefore necessary to consider a thick and weakly overdense plasma. According to condition (8) the plasma is transparent to the laser field, which ensures a strong interaction between electrons and a laser pulse.

B. Simulation parameters

We consider both linearly and circularly polarized laser pulses normally incident on a plasma layer of a variable thickness l surrounded by $100\lambda_L$ long vacuum regions on both sides. The initial electron density is $10 n_c$. The time is measured in laser periods $T_L = 2\pi/\omega_L$ and lengths are measured in laser wavelengths $\lambda_L = cT_L$. The laser energy fluence is $\mathcal{E}_L/n_c m_e c^3 T_L = \int_0^{t_{\mathrm{end}}} a_L^2 dt/T_L = 4 \times 10^5$ for the Gaussian laser pulse with $a_L = 200$ and the pulse duration of 14 T_L. The choice of these parameters is justified by conditions (14), (8), and (18). The laser pulse interacts with the target at $t = 0$. The total simulation time is $t_{\mathrm{end}} = 100\ T_L$. In the

simulations presented below three ion species are considered: protons, deuterons, and infinitely massive ions. These laser and plasma parameters constitute a new regime which has not been studied experimentally yet but will be available in near future.

The characteristic energies of laser plasma interaction are defined by the parameters $\eta_k = \mathcal{E}/\mathcal{E}_L$, where k stands for photon (γ), electrons (e), and ions (i): here, $\mathcal{E}_\gamma(t)$ is the energy fluence of the photons radiated up to the time t, $\mathcal{E}_e(t)$ is the electron energy per unit area at the time t. In a similar way, $\zeta_k = \mathrm{d}\eta_k/dt/T_L$ define the instantaneous relative radiation intensity and the energy absorption rate by the electrons and ions.

IV. ABSORPTION DEPENDENCE ON THE TARGET THICKNESS

The laser absorption depends strongly on the plasma thickness. This can be explained by the fact that the amplitude of the front surface positive electrostatic field increases with the target thickness (see Sec. II B). Thus, the electrons can gain more energy in the electrostatic field and radiate. The laser energy absorption depends also on the ion mass. Indeed, in a plasma with heavier ions the electrostatic field is stronger. This is demonstrated in Figure 1 where the radiation emission efficiency increases with the ion mass. In the case of a linear laser polarization, more than 80% of the laser energy is converted into the synchrotron radiation in the case of immobile ions whereas this ratio rises to ≈50% in the case of a proton plasma. However, this difference is almost two times bigger in the case of a circular laser polarization as it can be seen in Figure 1(c). A circular polarization and a plasma of light ions permit to have a maximum laser energy transfer to ions (see Figure 1(d)), yielding to less intense synchrotron radiation. We note that these values are in good agreement with those obtained with the QED approach (colored points) evoked in Sec. VII.

In the case of a thick target, $l = 100\lambda_L$ (see Figure 1(a)), the difference in the quantity of radiated energy between a deuteron and a proton plasma could be sufficient for experimental demonstration of the role of ion mass in the synchrotron radiation, in near future laser facilities.[3,34]

It is also important to analyze how the absorbed laser energy is distributed between electrons and ions. For a plasma of light ions, more than 10% of the incident laser energy can be transferred to ions for target thicknesses larger than 10 λ_L, whatever the laser polarization is, as it can be seen in Figure 1. In the case of a linear polarization, the ions do not have much impact on the energy transferred to electrons. This fact is due to the presence of the oscillating part of the ponderomotive force in the linear polarization case. Thus, the heating is the main energy source for electrons, which does not depend on the ion mass. The charge separation field tends to enhance the wave-particle interaction without any strong change of electron heating in the case of targets thicker than approximately 20 λ_L.

V. ELECTRON ACCELERATION

The goal of this section is to discuss the electron acceleration process and to make a link with the collective effects and the generation of synchrotron radiation.

The electron energy spectrum is less extended in the case of a plasma of immobile ions as it can be seen in Figure 2. For a thin target, the laser field penetrates throughout the target and carries away electrons by the ponderomotive force. Because the electrostatic pressure is relatively low, the target expands in forward and backward directions. Electron motion toward the laser is strongly affected by radiation losses, and their motion is reversed. Thereby, the electrons

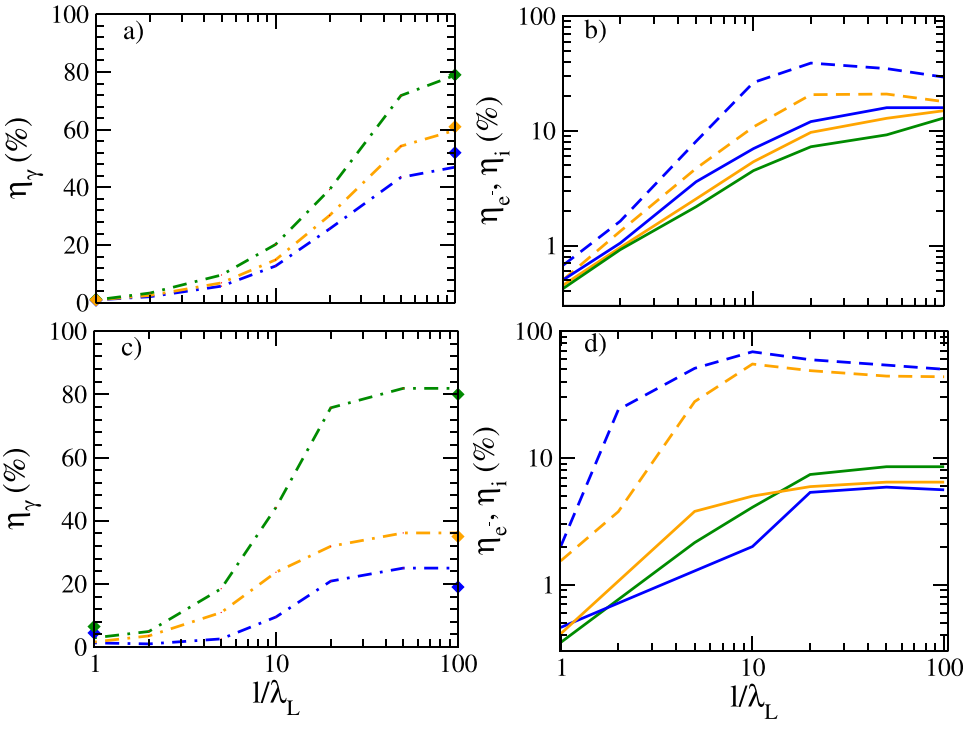

FIG. 1. Dependence of the laser energy conversion into photons η_γ (a) and (c), into electrons and ions η_e, η_i (b) and (d) as a function of the target thickness l for the plasma density $n_e = 10n_c$. Color code: blue, proton plasma; orange, deuteron plasma; green, plasma of immobile ions. The dashed lines–ions, full lines–electrons. (a) and (b) linear polarization. (c) and (d) circular polarization. The blue, orange, and green squares show the simulation data computed with the QED code CALDER described in Ref. 21.

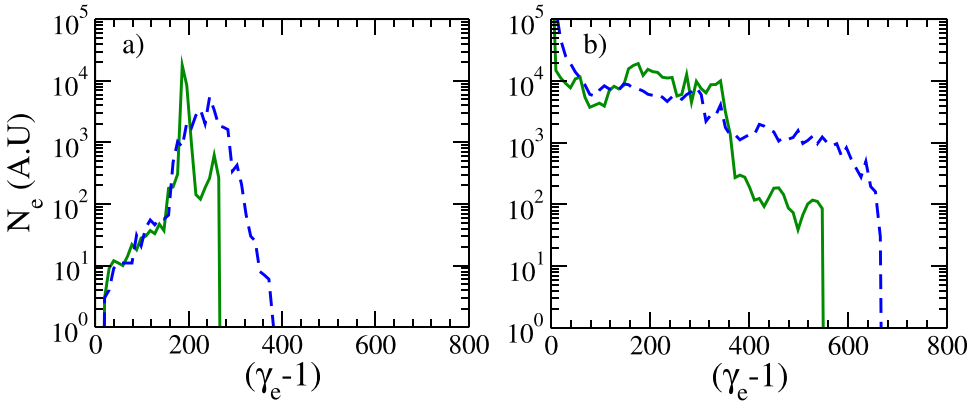

FIG. 2. Electron energy spectrum at the time of maximum synchrotron emission for $n_e = 10n_c$. Color code: green lines, plasma of immobile ions; dashed blues lines, proton plasma. (a) $l = 1\lambda_L$. (b) $l = 100\lambda_L$. A circular polarization is considered.

are forming a bunch in the energy distribution with the maximum at $\gamma_e \approx 200$ and $\gamma_e \approx 240$ in the case of a proton and fixed ions plasma, respectively. A stronger charge separation field, in the case of immobile ions corresponds to a stronger restoring force and to a 30% lower energy cutoff in the electron spectrum, as it can be seen in Figure 2(a). For a thick target, the electrostatic field can attain the same magnitude as the laser electric field. Then the electrons are gaining more energy and their cutoff energy increases almost two times, as it can be seen in Figure 2(b).

In order to better understand how collective effects affect the electron dynamics let us consider the orbit of an electron, having a kinetic energy close to the peak energy at the time of maximum synchrotron emission, $t_{\max}$ (see Figure 2).

For a thin target, because $E_s \ll E_L$, the laser field crosses the target and carries some electrons with it. These electrons oscillate in the laser field and are responsible for the synchrotron radiation emission. Besides, these electrons at the front of the laser pulse produce an electrostatic field which tends to transfer a part of the laser energy to protons (see Figure 1(d)). In the case of fixed ions, more energy is stored in the charge separation field, at the rear target side. Thereby, electrons accelerated at the front of the laser pulse can be further trapped by the electrostatic field (see Figure 3(a)) and strongly radiate when they go toward the laser. These features are further discussed in Sec. VI A where the temporal evolution of radiation is studied.

For a thick target, where $E_s \sim E_L$, the electron trajectories are more chaotic which means that the curvature radius $r_c \sim c/\omega_{re} \propto 1/\gamma_e$ is smaller, as it can be seen in Figure 3(b). That leads to stronger radiation losses and generation of higher-energy photons, as the electron rotation frequency is related to the critical frequency by $\omega_{re} = \frac{2}{3\gamma_e^3}\omega_{cr}$. This aspect is discussed in more detail in Sec. VI C. The increase of the ion mass leads to an increase of electric field E_s which further increases the synchrotron radiation.

VI. EFFECT OF THE ELECTROSTATIC FIELD ON RADIATION

A. Temporal behavior of the radiation

The radiated intensity attains a maximum at the time moment $t_{\max}$ which depends on the ion response time and the target thickness. As it can be seen in Figure 4(a) in the case of a thick target, the shape of the radiation pulse does not strongly depend on the ion mass. The most notable difference is in the amplitude of the radiation pulse which increases with the ion mass. The duration of the radiation pulse is longer than the laser pulse duration due the charge separation field E_s. In the case of a thin target ($l = 1\lambda_L$, see Figure 4(b)), the maximum amplitude of the radiation pulse increases with the ion mass but the duration of radiation emission is longer for a proton plasma. As it is explained in Sec. V, in the case of a plasma of immobile ions the synchrotron radiation generation is mainly due to the electrons which propagate with the laser pulse, and are trapped in the charge separation field. Thereby the frequency of radiation and its intensity increase as the electron propagates toward the laser. On the contrary, for a proton plasma the electrons accelerated at the front of the laser pulse are much less affected by the electrostatic field. Thereby, they can radiate for a longer

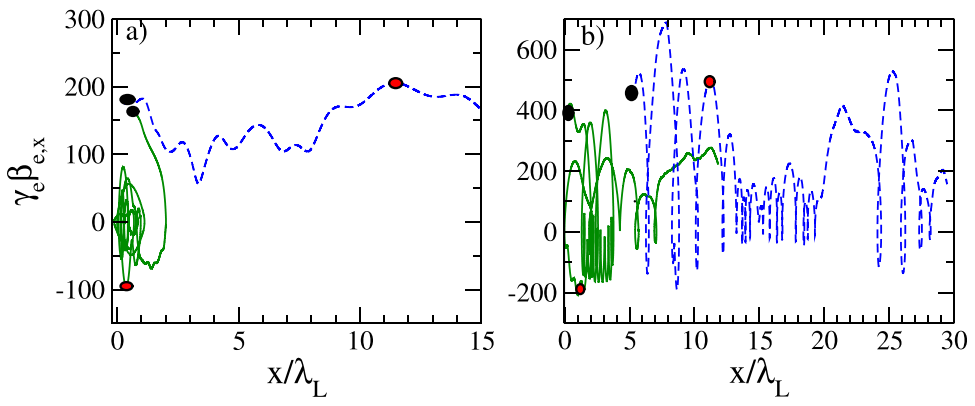

FIG. 3. Phase orbit of an electron over the time interval $t \in [t_{\max} - 20T_L; t_{\max} + 20T_L]$ for $n_e = 10n_c$. Color code: green lines, plasma of immobile ions; dashed blue lines, proton plasma. (a) $l = 1\lambda_L$. (b) $l = 100\lambda_L$. The electron position at the time of maximum synchrotron emission is represented by a red point. The electron initial position is marked by a black point. A circular polarization is considered.

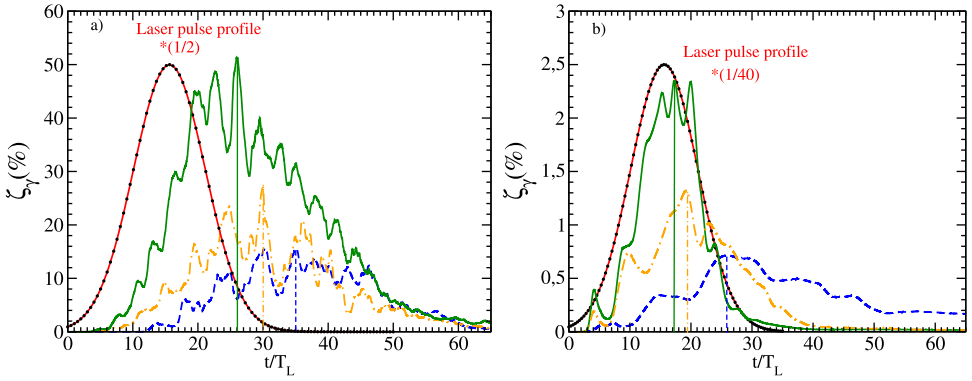

FIG. 4. Total radiated intensity versus time for a thick and a thin target (a) $l = 100\lambda_L$ and (b) $l = 1\lambda_L$. Color code: blue lines, proton plasma; in orange, deuteron plasma; in green, plasma of immobile ions. The emission time $t_{\max}$ is shown with vertical dashed lines whose color corresponds to the ion species of the plasma.

time in the laser field, as it can be seen in Figure 4(b). As these electrons propagate with the laser pulse, the frequency and the intensity of radiation are lower, which explains why the radiated intensity at every time is much lower in a proton plasma. Despite these differences on the shape of the radiated pulse, the total radiated energy in the case of a thin target shows a weak dependence on the ion mass.

B. Spatial behavior of the radiation

We define the characteristic length $l_{\rm rad}$ as the size of emission zone at the time $t_{\max}$. For laser-plasma interactions with $a_L \gg n_e/n_c$, the length $l_{\rm rad}$ depends on the rise time of the laser field, $T_{\rm rise}$. The electrostatic field can strongly modify the radiation emitted by electrons if the rise time of the laser pulse is larger than the response time of ions (see Ref. 13), $T_i \sim 2\pi/\omega_{pi}$ where $\omega_{pi} = (Z^2e^2n_i/m_i\epsilon_0)^{1/2}$ is the ion frequency. This conditions reads

$$T_{\rm rise} \geq T_i. \tag{18}$$

For a linear polarization, the length $l_{\rm rad}$ is comparable to the distance traveled by relativistic electrons during the time $T_{\rm rise}$. For a circular polarization, the radiation length is shorter as more laser energy is transferred to ions and the electrostatic field is stronger. According to the simulation results, the length $l_{\rm rad} = cT_{\rm rise}\mathcal{F}(\mathrm{Max}[\alpha])$ can be described by the following empirical relation:

$$\mathcal{F}(\mathrm{Max}[\alpha]) = \begin{cases} 1 \text{ for a linear polarization} \\ \dfrac{\mathrm{Max}[\alpha]}{2} \text{ for mobile ions and } l \gg \lambda_L \\ \mathrm{Max}[\alpha] \text{ for immobile ions and } l \gg \lambda_L \\ \sqrt{\mathrm{Max}[\alpha]} \text{ for } l \sim \lambda_L. \end{cases} \tag{19}$$

The function $\mathcal{F}(\mathrm{Max}[\alpha])$ is an increasing function of the plasma length and the ion mass. It is equal to its maximum value of 1 for the linear polarization and of the order of α for the circular polarization in a thick plasma. In the case of the piston regime (see Ref. 35), and for mobile ions, the maximum amplitude of the charge separation field can be estimated as

$$\mathrm{Max}[\alpha] \simeq 2\left(\frac{1}{1+2B}\right)^{1/2}. \tag{20}$$

Then, using expressions (11) and (19) we can express the total radiated energy per surface unit as

$$\mathcal{E}_\gamma(t\to\infty) \simeq 6(\omega_L T_{\rm rise})(\omega_L\tau_r)\frac{n_e}{n_c}\mathcal{F}(\mathrm{Max}[\alpha])a_L^2\frac{1}{\tau_L} \times \int_0^\infty \left[g(t)+\alpha(t)^2\right]^2 dt\mathcal{E}_L, \tag{21}$$

where $\mathcal{E}_L = \tau_L I_L$ is the laser fluence.

The higher is the ion mass, less energy is transferred to ions, leading to a more radiation.

It is possible to evaluate the term $\int_0^\infty [g(t)+\alpha(t)^2]^2 \mathrm{dt}$ by assuming $\alpha(t)^2 \simeq \mathrm{Max}[\alpha^2]$ during the time $T_{\rm rise}$: $\int_0^\infty [g(t)+\alpha(t)^2]^2 \mathrm{dt} = \frac{\tau_L}{\sqrt{2}} + \mathrm{Max}[\alpha^2]T_{\rm rise}\left[\frac{1}{\sqrt{2}} + \frac{\tau_L}{\sqrt{\tau_L^2+T_{\rm rise}^2}}\right]$. In the case of a thick target ($\mathrm{Max}[\alpha] \sim 1$) and $T_{\rm rise} \simeq \tau_L$, the radiated energy $\mathcal{E}_\gamma$ is increased by a factor of 3 compared to a thin target where $\mathrm{Max}[\alpha] \ll 1$. Moreover, for $T_{\rm rise} \ll \tau_L$, the electrostatic field has no influence on the synchrotron radiation (see Eq. (21)), which is consistent with the inequality (18).

Figure 5 illustrates the spatial distribution of the electrostatic field and the radiated power. In each case, the characteristic length $l_{\rm rad}$ is comparable with the localization length of the electrostatic field. Furthermore, the fluence of emitted radiation depends on this length according to Eq. (21). The estimates of $l_{\rm rad}$ (19) agree with the simulation results. For instance, in the case of a circular polarization and a thick target, we get $l_{rad} \simeq 10.5\lambda_L$ and $\simeq 4.7\lambda_L$ for a proton plasma and a plasma of immobile ions, respectively, which is in good agreement with Figure 5(c).

C. γ-ray emission

This section is devoted to the analysis of radiation emission as a function of the target thickness and of the ion mass. For clarity we first consider effects coming from the target thickness and second those related to the ion mass.

In a general point of view, the radiation spectrum is extended to higher energies due the fact that the electrostatic field decreases the curvature radius of the radiating electrons

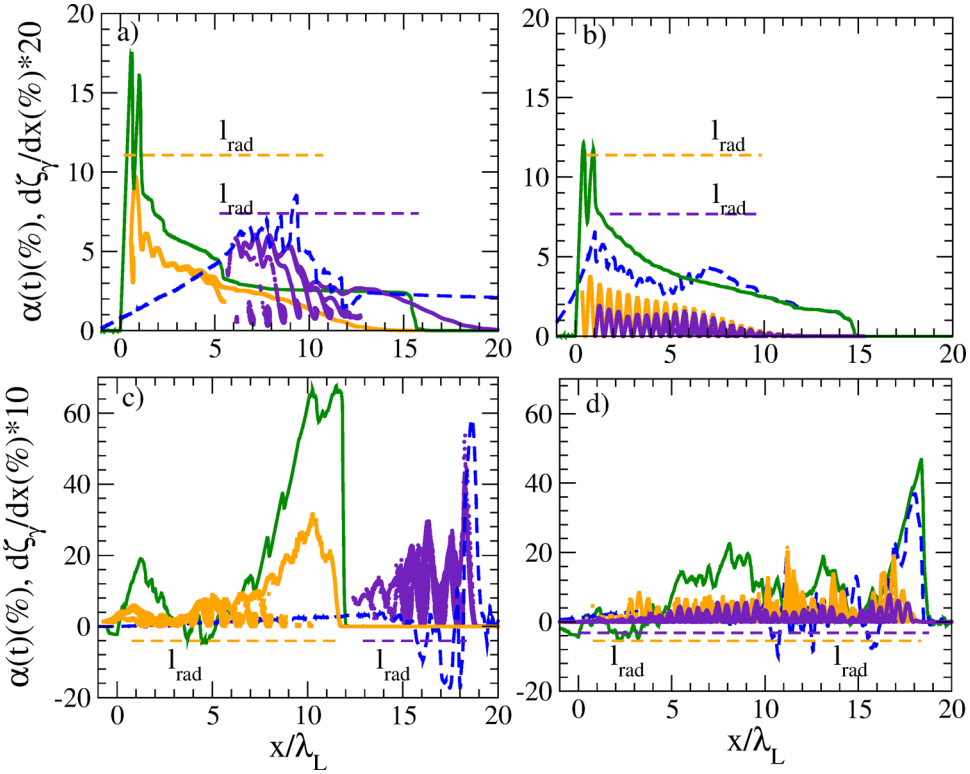

FIG. 5. Field ratio $\alpha(t) \equiv E_s(t)/E_L$ and the photon conversion efficiency spatial distribution $\zeta_\gamma(\%)$ at the time of maximum synchrotron emission. Code color for the front charge separation field: in green, plasma of immobile ions; dashed blue lines, proton plasma. Color code for ζ_γ: purple circles, proton plasma; yellow squares, plasma of immobile ions. (a) and (b) $l = 1\lambda_L$; (c) and (d) $l = 100\lambda_L$. The cases of a circular polarization (a) and (c) and a linear polarization (b) and (d) are considered.

(see Sec. V). By comparing the panels corresponding to the thin and thick target cases (see Figures 6(a)–6(d)) we conclude that the charge separation field contributes to generation of photons with energies larger than $\sim 2a_L m_e c^2$. For a circular polarization, the charge separation field increases the characteristic photon energy by a factor of 3, which is consistent with Eq. (21).

1. Effects coming from the target thickness

For a thin target, because $E_s \ll E_L$, the Lorentz force can be evaluated as: $\mathbf{F}_{Le} \sim m_e c\omega_L\, \mathbf{a}_L$. Thereby, the average characteristic frequency can be estimated as $\langle \omega_{cr} \rangle \sim \gamma_e^2 a_L \omega_L \approx 10^7 \omega_L$ which is in good agreement with Figure 7. In the case of a circular polarization, the distribution of critical frequencies is more anisotropic compared to the linear case, see Figure 7(a). It is mostly concentrated in an interval $\Delta\theta \in [0°, 90°] \cup [270°, 360°]$. In this case, $p_{e,z} \sim p_{e,y}$ which implies that $p_\parallel < p_\perp$. Therefore, the synchrotron radiation is mostly emitted at the rear of the expanded target. In the case of a linear polarization, there is no strong dependence of the synchrotron radiation emission over θ, which means that synchrotron radiation is mainly generated by hot electrons strongly oscillating in the laser field. For a thick target, the electrostatic field plays an important role in electron acceleration with noticeable consequences for emitted radiation. The electrostatic field spreads the radiation spectrum to lower frequencies because electrons can radiate for a longer time. However, high energy photons with $\hbar\omega_{cr} \geq 10^7 \hbar\omega_L \approx 10\,\text{MeV}$ are generated by ultra-relativistic electrons accelerated both in the electrostatic and the laser electric fields. In the case of a linear polarization, this effect is even more spectacular due to enhancement of the electron heating, which shows that the most energetic part of the synchrotron radiation is emitted at $\theta \approx 0°$. It corresponds to the propagation direction of the hot electrons.

2. Effects coming from the ion mass

Unlike previous situations, for a thick target and a linear polarization (see Figure 6(d)), the photon spectrum of a proton plasma is more extended to high energies. This part of the photon spectrum is due to electrons propagating in front of the laser pulse and strongly heated by the oscillating part of the ponderomotive force. They acquire a strong momentum while crossing the piston interface (see Ref. 35) and then, propagating toward the laser pulse. They lose much of their kinetic energy to the radiation and return back to the piston interface (see Ref. 8). The linear polarization removes the ion mass effect on the intense synchrotron radiation as it can be seen in Figures 7(b) and 7(d). However, in the case of a thick target and a circular polarization, a plasma of fixed ions yields a strong radiation at $\theta \approx 180°$, featuring a strong influence of the electrostatic field on the synchrotron radiation. Thereby, the electrostatic field increases the number of backward propagating electrons. This feature is confirmed by comparing electron and photon energy distributions in Figures 2 and 6. For a thick target, the effect of ion mass, on the energy gain of electrons can be estimated as

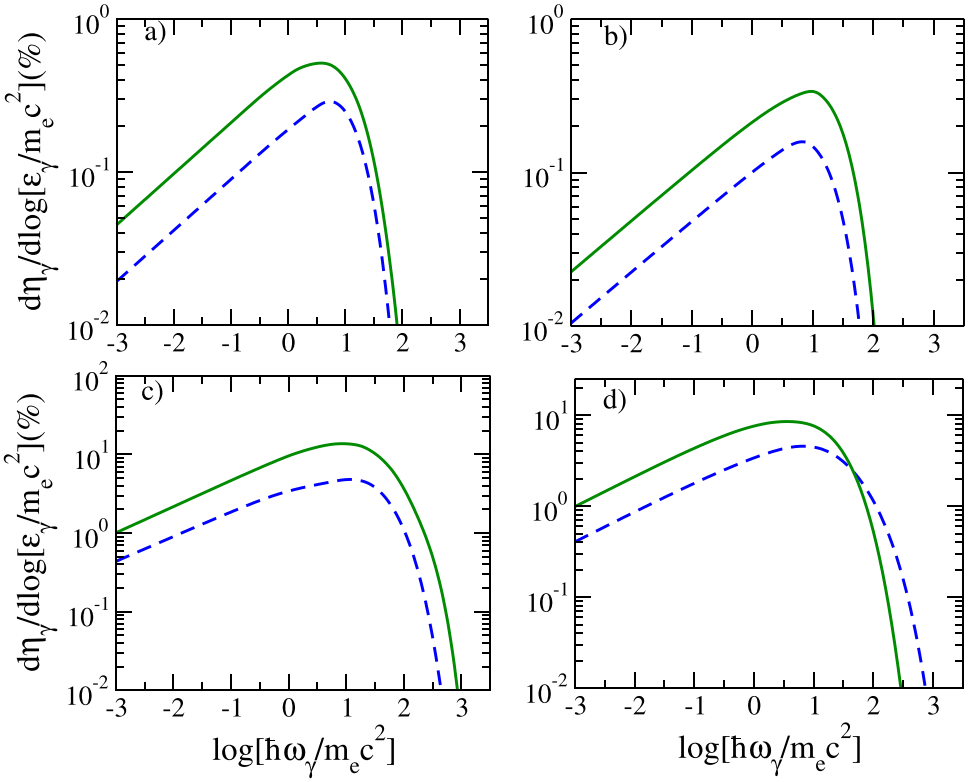

FIG. 6. Photon energy spectrum at the time of maximum synchrotron emission. Color code: solid green lines, plasma of immobile ions; dashed blue lines, proton plasma. (a) and (b) $l = 1\lambda_L$. (c),(d): $l = 100\lambda_L$. (a) and (c) circular polarization. (b) and (d) linear polarization.

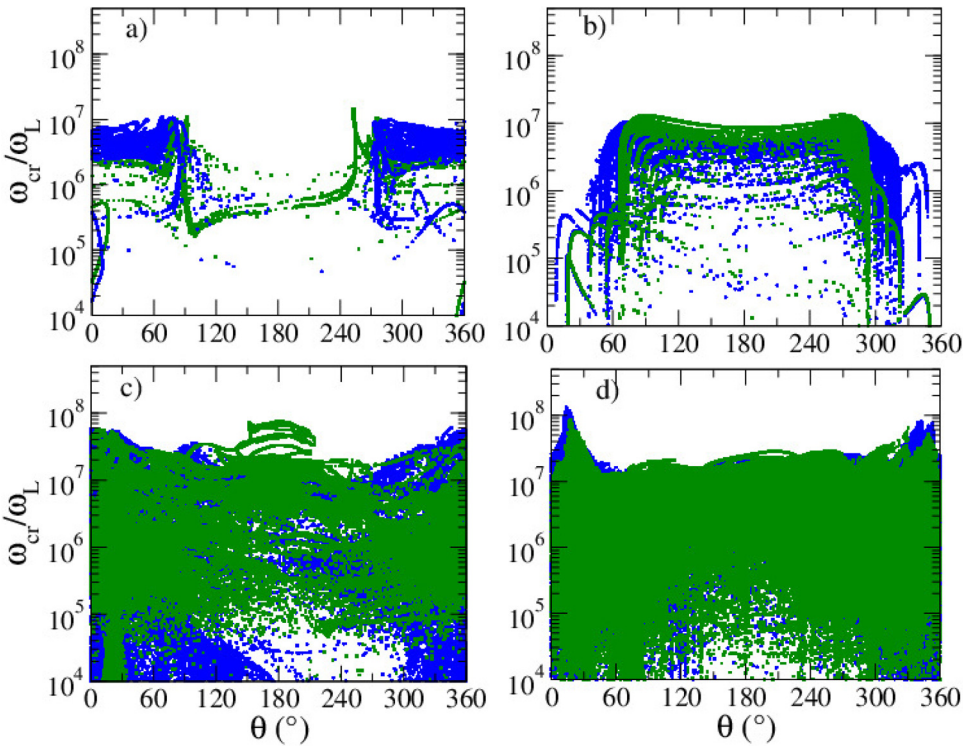

FIG. 7. Distribution of the critical frequencies associated to radiation with respect to θ at the maximum synchrotron emission. Color code: green squares, plasma of immobile ions; blue circles, proton plasma. (a) and (b) $l = 1\lambda_L$. (c) and (d) $l = 100\lambda_L$. (a) and (c) circular polarization. (b) and (d) linear polarization.

$$\Delta\gamma_{e,\mathrm{hot}}[m_{i,1} \rightarrow m_{i,2}] = \frac{\Theta\gamma_{e,\mathrm{hot}}[m_{i,2}]}{\Theta\gamma_{e,\mathrm{hot}}[m_{i,1}]}, \tag{22}$$

where

$$\Theta\gamma_{e,hot}[m_{i,o}] \sim \sqrt{\frac{\mathrm{Max}[\alpha]_{\{o\}}}{\mathcal{F}\left(\mathrm{Max}[\alpha]_{\{o\}}\right)}} \tag{23}$$

accounts for the effect of electrostatic field. For a circular polarization the expressions (19), (22), (23) with the values of α (7) taken from Figure 5(c) predict the increase of electron energy $\Delta\gamma_{e,\mathrm{hot}}[m_{i,\infty} \rightarrow m_{i,\mathrm{protons}}] \simeq 1.4$. This is close to results shown in Figure 2(b).

VII. DISCUSSIONS

In order to confirm the validity of our classical approach, the results have been compared with the PIC code CALDER using a QED Monte-Carlo model of radiation implemented by Lobet *et al.*[21] The comparison is made in the cases of a linear and circular polarization, for two target thicknesses of 1 and 100 λ_L, with the same laser parameters, that is, a Gaussian pulse having a peak intensity of $1.1 \times 10^{23}\,\mathrm{W/cm^2}$ and a duration of $14T_L$. Other parameters remain unchanged. As shown in Figure 1, the simulations with two codes, PICLS and CALDER, give very similar results for our set of parameters, which confirm that a classical treatment is appropriate in our regime of interaction. The time-evolution of the percentage of electron with a quantum parameter χ_e up to 0.1 and 0.2 is shown in Fig. 8.

The electrons of large quantum parameters are concentrated at the laser-solid interface where the space-charge separation is significant and the particles are strongly accelerated forward by the laser ponderomotive force. As a consequence, the percentage of electrons with high χ_e values is higher for thin targets and decreases by dilution effect with thicker plasmas. For thin targets ($l \sim 1\lambda_\mathrm{L}$), the electrons are accelerated by the laser radiation pressure so that a significant part of them can reach χ_e values close to 0.1 but only a very few particles can go up to χ_e of 0.2. For the thickest target ($l \sim 100\lambda_\mathrm{L}$), the proportion of high-χ_e electrons is diluted with the low-energy electrons of the plasma, around few percents for $\chi_e > 0.1$ and the population of electrons with $\chi_e > 0.2$ drops dramatically. Thus, the classical approach can be used for any combination of parameters at this laser intensity. This is in good agreement with previous studies reported in Refs. 36 and 37. The number of very energetic electrons depends also on the ion mass. The higher the ion mass, the larger the population of high-χ_e due to the stronger charge-separation fields at the laser-solid interface.

The detection of the ion mass effect could be feasible in near future by measuring the angular distribution of the emitted radiation and the total amount of laser energy converted into intense synchrotron radiation. Recently, a multichannel scintillating electron detector has been developed by Gray (see Ref. 38) which includes 30 individual channels placed in 20° intervals at the front of the target and in 5° intervals at the rear of the target. The scintillator is sensitive to almost all types of ionizing radiation. One can experimentally differentiate between the species by using a magnetic field to bend the charged particles. This detector could be used on future ultra-intense laser facilities for measuring the electrons and photons with energies extending up to 100 MeV.

In conclusion, we have shown that the γ-ray emission from a laser driven plasma is enhanced by charge separation field, in the radiation dominated regime. The electrostatic

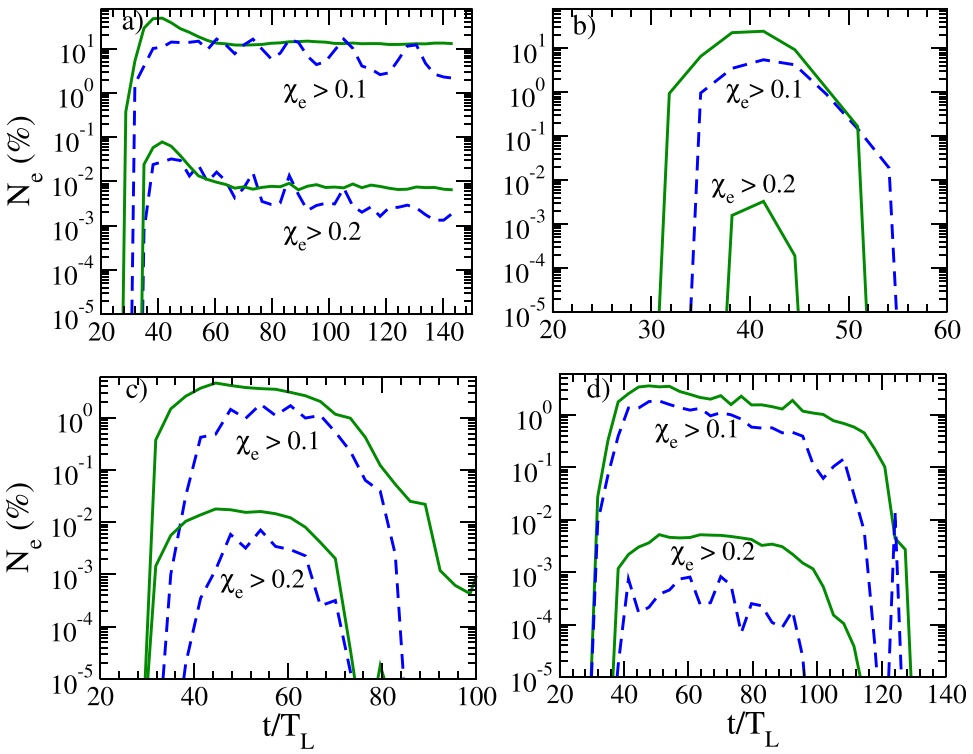

FIG. 8. Percentage of electrons having the quantum parameter $\chi_e > 0.1$ and $\chi_e > 0.2$ over time computed from QED approach presented in Ref. 21. Color code: solid green lines, plasma of immobile ions; dashed blue lines, proton plasma. (a) and (b) $l = 1\lambda_L$. (c) and (d) $l = 100\lambda_L$. (a) and (c) circular polarization. (b) and (d) linear polarization.

field enables a higher conversion of the laser energy into an intense radiation and extends the photon spectra to higher energies. If the electrostatic field amplitude is close to that of the laser field the radiated fluence can be increased three times compared to the case where the electrostatic field is negligible. One may expect a photon emission with energies up to a few hundred MeV in the case of a thick target. The electrostatic field depends on the ion mobility and target thickness, and it affects strongly the direction of emitted radiation due to a strong modification of the electron trajectory. Besides, the ion mass affects the laser energy distribution between hot electrons and intense synchrotron radiation.

The influence of the charge separation field on the synchrotron radiation can be demonstrated in experiments with solid hydrogen targets which have an electron density of the order of $10n_c$ for a laser wavelength of 1 μm. This can be evaluated by measuring the angular distribution of the radiation and the total radiated energy.

ACKNOWLEDGMENTS

We thank Professor Yasuhiko Sentoku for usage of the code PICLS. We thank Dr. Ross Gray for fruitful discussions. Support from the Aquitaine Regional Council, the ANR SILAMPA, and EPSRC (Grant No. EP/J003832/1) was also acknowledged.

[1]T. Esirkepov, M. Borghesi, S. V. Bulanov, G. Mourou, and T. Tajima, Phys. Rev. Lett. **92**, 175003 (2004).
[2]A. Di Piazza, K. Z. Hatsagortsyan, and C. H. Keitel, Phys. Rev. Lett. **102**, 254802 (2009).
[3]See http://www.extreme-light-infrastructure.eu/ for ELI project.
[4]H. Daido *et al*., Rep. Prog. Phys. **75**, 056401 (2012); A. Macchi *et al*. Rev. Mod. Phys. **85**, 751 (2013) and references therein.
[5]A. Zhidkov, J. Koga, A. Sasaki, and M. Uesaka, Phys. Rev. Lett. **88**, 185002 (2002).
[6]J. Koga, T. Zh. Esirkepov, and S. V. Bulanov, Phys. Plasmas **12**, 093106 (2005).
[7]M. Tamburini, F. Pegoraro, A. Di Piazza, Ch. H. Keitel, and A. Macchi, New J. Phys. **12**, 123005 (2010).
[8]N. Naumova, T. Schlegel, V. T. Tikhonchuk, C. Labaune, I. V. Sokolov, and G. Mourou, Phys. Rev. Lett. **102**, 025002 (2009).
[9]M. Tamburini, F. Pegoraro, A. DiPiazza, C. H. Keitel, T. V. Liseykina, and A. Macchi, Nucl. Instrum. Meth. A **653**, 181 (2011).
[10]M. Chen, A. Pukhov, T. P. Yu, and Z. M. Sheng, Plasma Phys. Control. Fusion **53**, 014004 (2011).
[11]R. Capdessus, E. d'Humières, and V. T. Tikhonchuk, Phys. Rev. E **86**, 036401 (2012).
[12]C. S. Brady, C. P. Ridgers, T. D. Arber, A. R. Bell, and J. G. Kirk, Phys. Rev. Lett. **109**, 245006 (2012).
[13]R. Capdessus, E. d'Humières, and V. T. Tikhonchuk, Phys. Rev. Lett. **110**, 215003 (2013).
[14]G. Lehmann and K. H. Spatschek, Phys. Rev. E **85**, 056412 (2012).
[15]C. Cremaschini and T. Tessarotto, Phys. Rev. E **87**, 032107 (2013).
[16]A. Noble, D. A. Burton, J. Gratus, and D. A. Jaroszynski, J. Math. Phys. **54**, 043101 (2013).
[17]D. A. Burton and A. Noble, Phys. Lett. A **378**, 1031–1035 (2014).
[18]C. P. Ridgers, C. S. Brady, R. Duclous, J. G. Kirk, K. Bennett, T. D. Arber, A. P. L. Robinson, and A. R. Bell, Phys. Rev. Lett. **108**, 165006 (2012).
[19]M. Vranic, J. L. Martins, J. Vieira, R. A. Fonseca, and L. O. Silva, Phys. Rev. Lett. **113**, 134801 (2014).
[20]A. G. R. Thomas, C. P. Ridgers, S. S. Bulanov, B. J. Griffin, and S. P. D. Mangles, Phys. Rev. X **2**, 041004 (2012).
[21]M. Lobet, E. d'Humières, M. Grech, C. Ruyer, X. Davoine, and L. Gremillet, "Modeling of radiative and quantum electrodynamics effects in PIC simulations of ultra-relativistic laser-plasma interaction," J. Phys.: Conf: Ser. (to be published); e-print arXiv:1311.1107.
[22]P. A. M. Dirac, Proc. R. Soc. London, Ser. A **167**, 148 (1938).
[23]I. V. Sokolov, J. Exp. Theor. Phys. **109**, 207 (2009).
[24]L. D. Landau and E. M. Lifschitz, *The Classical Theory of Fields*, 4th ed. (Pergamon, New York, 1994), vol. 2.
[25]R. Duclous, J. G. Kirk, and A. R. Bell, Plasma Phys. Control Fusion **53**, 015009 (2011).
[26]N. V. Elkina, A. M. Fedotov, I. Yu. Kostyukov, M. V. Legkov, N. B. Narozhny, E. N. Nerush, and H. Ruhl, Phys. Rev. ST Accel. Beams **14**, 054401 (2011).
[27]A. I. Nikishov and V. I. Ritus, Sov. Phys. JETP **19**, 5 (1964).
[28]A. I. Nikishov and V. I. Ritus, Sov. Phys. JETP **29**, 1 (1969).
[29]A. Macchi, S. Veghini, and F. Pegoraro, Phys. Rev. Lett. **103**, 085003 (2009).
[30]I. V. Sokolov, N. M. Naumova, and J. A. Nees, Phys. Plasmas **18**, 093109 (2011).
[31]S. C. Wilks, W. L. Kruer, M. Tabak, and A. B. Langdon, Phys. Rev. Lett. **69**, 1383 (1992).
[32]J. D. Jackson, *Classical Electrodynamics*, 3rd. ed. (Wiley, New York, 1999).
[33]Y. Sentoku and A. Kemp, J. Comput. Phys. **227**, 6846 (2008).
[34]See https://www.stfc.ac.uk/76.aspx forRutherford Appeleton Laboratory website.
[35]T. Schlegel, N. Naumova, V. T. Tikhonchuk, C. Labaune, I. V. Sokolov, and G. Mourou, Phys. Plasmas **16**, 083103 (2009).
[36]A. R. Bell and J. G. Kirk, Phys. Rev. Lett. **101**, 200403 (2008).
[37]C. P. Ridgers, C. S. Brady, R. Duclous, J. G. Kirk, K. Bennett, T. D. Arber, and A. R. Bell, Phys. Plasmas **20**, 056701 (2013).
[38]R. Gray, "*On Mechanisms of Laser*-Coupling *to Fast Electrons in Ultraintense Laser*-Solid Interactions," Ph.D. thesis, University of Strathclyde, U.K, 2013.